THE JOURNAL OF BIOLOGICAL CHEMISTRY

Vol. 269, No. 13, Issue of April 1, pp. 9610-9619, 1994
Printed in U.S.A.

Membrane-induced Helical Conformation of an Active Candidacidal Fragment of Salivary Histatins*

(Received for publication, November 30, 1993)

Periathamby Antony Raj‡, Sunil-Datta Soni, and Michael J. Levine

From the Department of Oral Biology and the Dental Research Institute, State University of New York at Buffalo, Buffalo, New York 14214

The conformational preference of the candidacidal C-terminal 16 residue fragment (9–24; G-Y-K-R-K-F-H-E-K-H-H-S-H-R-G-Y) of salivary histatin 5 was examined in water, methanol, and dimethyl sulfoxide solutions using 500 MHz two-dimensional-NMR. Fourier transform infrared and CD spectroscopy were used to delineate its membrane-bound conformation in lipid vesicles. The peptide backbone and side-chain proton resonance assignments were accomplished by two-dimensional total correlated and nuclear Overhauser effect (NOE) spectra. The coupling constant ($J_{NH\text{-}C\alpha_H}$) values determined from the double quantum-filtered correlated spectra, temperature coefficients of NH chemical shifts (dδ/dT), $^1H/^2H$ exchange rates on amide resonances, and the set of NOE connectivities were used to delineate backbone conformational features. The high $J_{NH\text{-}C\alpha_H}$ values (≥7.4 Hz), absence of any characteristic NH-NH (*i*, *i*+1) or $C^\alpha H\text{-}C^\beta H$ (*i*, *i*+3) NOE connectivities, high dδ/dT values (≥0.004), and the fast $^1H/^2H$ amide exchange suggest that the histatin peptide favors unfolded random conformations in aqueous solution at pH 3.8. In contrast, the $J_{NH\text{-}C\alpha_H}$ values (≤6.5 Hz), slow $^1H/^2H$ exchange, low dδ/dT values (≤0.003) observed for amide resonances of residues 5–16, and the characteristic NH-NH (*i*, *i*+1), $C^\alpha H\text{-}C^\beta H$ (*i*, *i*+3) NOE connectivities, provide evidence for the presence of largely α-helical conformations in dimethyl sulfoxide, which mimics the polar aprotic membrane environment. In methanolic solutions, 3_{10}-helical conformations could exist as a minor population together with the major α-helical conformations. Fourier transform infrared spectroscopy and CD data indicate that lipid environments such as dimyristoylphosphatidylcholine vesicles could induce the peptide to fold into predominantly α-helical conformation. The results suggest that in dimethyl sulfoxide and dimyristoylphosphatidylcholine vesicles the candidacidal domain of salivary histatin 5 prefers a largely helical conformation, which could facilitate its interaction with the membrane of *Candida albicans*. The mechanism of antimicrobial action of this class of polypeptides appears to involve primarily electrostatic and hydrogen-bonding interaction of cationic and polar residues with the head groups of the plasma membranes of target cells.

Histatins are a family of related neutral and basic histidine-rich peptides present in human parotid and submandibular-sublingual secretions (1–3). They can be involved in the formation of acquired enamel pellicle and participate in the mineral-solution dynamics of the oral fluids (4–6). The histidine-rich proteins in saliva enhance the glycolytic activity of certain oral microorganisms (7), possess antimicrobial activity against a few strains of *Streptococcus mutans* (8, 9), and inhibit hemagglutination of *Porphyromonas gingivalis* (10, 11) and coaggregation between *P. gingivalis* and *Streptococcus mitis* (12). Importantly, these polypeptides have been shown to exhibit remarkable growth-inhibitory effects on *Candida albicans* presumably by altering membrane permeability and causing membrane damage (2, 9, 13–15). Histatins have also been reported to inhibit germination of *C. albicans* at the physiological concentration in salivary secretions (5, 16). The multifunctional properties of salivary histatins have led to the isolation, separation, purification, and functional characterization of this family of peptides (6, 17–20).

Twelve salivary histatins have been isolated from saliva and their primary structures (Fig. 1) determined (2, 18). Among the twelve histatins described so far, histatin 1 and histatin 3 have been shown to arise from different structural genes, while the smaller histatins originate from post-translational proteolysis (2, 21). It has been recently suggested that histatin 5 might be derived from a distinct mRNA and not by proteolytic processing of histatin 3 (22). The candidacidal potency of the major histatins has an inverse relationship to their molecular size, with histatin 5 being the most and histatin 1 the least effective (18).

Despite the obvious importance of salivary histatins in the nonimmune oral host defense system, there are only a very few reports on the secondary structure and structure/function analyses of these bioactive peptides. Previously, we have studied the candidacidal activity of histatin 5 and its fragments (23). The candidacidal activity of the fragments was dependent on sequence, chain length, and their ability to adopt helical conformation in hydrophobic media. The results suggested that the candidacidal activity of histatin 5 was localized to the C-terminal 16 residue sequence. Although the conserved region in most of the basic histatins (*e.g.* histatin 3-histatin 10) appears to be K-F-H-E-K-H-H-S-H-R-G-Y (Fig. 1), the cidal potency of this 12 residue sequence was much less as compared with histatin 5. However, increasing the chain length to 16 residues (G-Y-K-R-K-F-H-E-K-H-H-S-H-R-G-Y) resulted in a fragment (C16)[1] that retained the activity of the parent histatin 5 (23).

Salivary histatins, being polar and hydrophilic, appear distinctly different from other cationic antimicrobial and mem-

* This work was supported by United States Public Health Service Research Grants DE07585 and DE08240. The costs of publication of this article were defrayed in part by the payment of page charges. This article must therefore be hereby marked "*advertisement*" in accordance with 18 U.S.C. Section 1734 solely to indicate this fact.

‡ To whom correspondence should be addressed. Tel.: 716-829-2114; Fax: 716-829-3942.

[1] The abbreviations used are: C16, C-terminal 16 residue fragment (9–24) of salivary histatin 5; ATR, attenuated total reflectance; CD_3OH, deuterated methanol; $(CD_3)_2SO$, deuterated dimethyl sulfoxide; CIR, cylindrical internal reflectance; 1D and 2D, one- and two-dimensional; DMPC, dimyristoylphosphatidylcholine; DQF-COSY, double quantum-filtered correlated spectroscopy; FTIR, Fourier transform infrared spectroscopy; ^2H_2O, deuterated water; NOE, nuclear Overhauser effect; NOESY, NOE spectroscopy; TOCSY, total correlated spectroscopy; TMP, trimethyl phosphate.

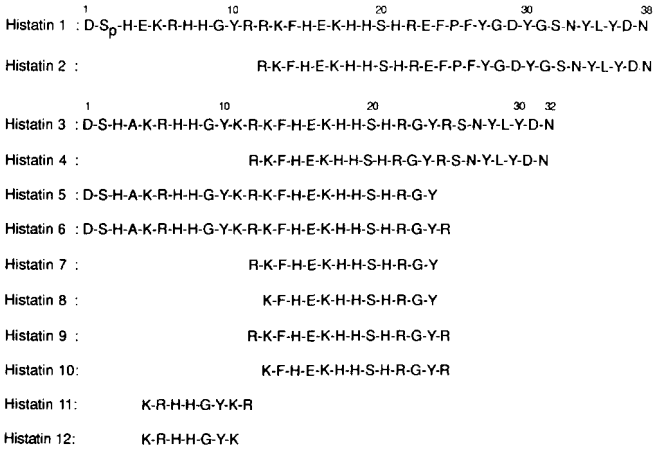

FIG. 1. **Amino acid sequences of salivary histatins.** The *one letter symbols* used for amino acids in the sequences are described as in IUPAC-IUB Commission on Biochemical Nomenclature (71). S_p represents phosphoserine.

brane-active polypeptides such as magainins, defensins, and tachyplesins, which have been shown to form amphiphilic α-helical or β-sheet structures (24–27). The C16 fragment represents the functional domain for candidacidal activity and is a conserved region of many of the histatins. This peptide was examined by 500 MHz 2D proton NMR in both aqueous and organic solutions to delineate the influence of solvent polarity, hydrophobicity, and hydrogen-bonding potency on the backbone conformation. In addition, Fourier transform infrared (FTIR) and CD spectroscopy have also been used to complement the NMR data and to determine the conformation of this active sequence in dimyristoylphosphatidylcholine (DMPC) vesicles.

EXPERIMENTAL PROCEDURES

Peptide Synthesis and Purification—The C16 was synthesized by solid-phase procedures, purified by high performance liquid chromatography, and tested for its homogeneity by analytical high performance liquid chromatography, amino acid, and sequence analysis as described previously (23).

NMR Sample Preparation—The purified peptide (7 mg) was dissolved in 630 µl of double distilled water and 70 µl of ^2H_2O (Cambridge Isotope Laboratories, Woburn, MA), the peptide concentration being ~5 mM. The pH of the aqueous peptide solution was found to be 3.8. For the NMR experiments in dimethyl sulfoxide and methanol, the peptide (7 mg) was dissolved in 700 µl of 99.9% $(CD_3)_2SO$ (Cambridge Isotope Laboratories) and 99.8% CD_3OH (MSD Isotopes, Montreal, Canada), respectively. All 1D and 2D NMR experiments used for conformational analyses were performed at 30 °C in these solvents.

NMR Measurements—All NMR experiments were carried out at 500 MHz on a Varian VXR-500 spectrometer equipped with a SUN Sparc station 2. The 1D-NMR spectra were recorded with a spectral width of 5000 Hz and a relaxation delay time of 2.5 s using 8-K data points zero filled to 32 K before Fourier transformation. All 2D spectra were acquired in the phase-sensitive absorption mode with quadrature detection in both dimensions using the hypercomplex method (28). Typically, 2048 complex data points during the acquisition time (t_2) and 256–512 complex free induction decays during the evolution period (t_1) with a total of 48–64 transients for each free induction decay were collected. The spectral width in both dimensions was 4500 Hz for the 500 MHz data. The solvent signals of water and methanol were suppressed by low power irradiation of the resonances at all times except during t_1 and t_2. All 2D experiments were multiplied by a phase-shifted sine bell function in both dimensions and zero filled before Fourier transformation to achieve appropriate resolution in each dimension. The NOESY, DQF-COSY, and TOCSY experiments were performed using standard methods (29–35). The TOCSY experiments were recorded using a MLEV-16 pulse sequence for the spin lock (33) with a field strength of approximately 5.6 kHz and a trim pulse of 2 ms using an isotropic mixing period of 65 ms for H_2O and CD_3OH and 75 ms for $(CD_3)_2SO$. The 2D NOE experiments were acquired with several mixing times ranging from 50 to 350 ms. The intensities of the NOE cross-peaks were measured as a function of mixing time and found to be roughly linear up to 150, 300, and 250 ms in H_2O, CD_3OH, and $(CD_3)_2SO$, respectively, suggesting that spin diffusion is not significant in the range of mixing times for these solvents. All NOE experiments described were therefore performed with a mixing time of 150, 300, and 250 ms in H_2O, CD_3OH, and $(CD_3)_2SO$, respectively.

The coupling constant ($J_{NH\text{-}C^\alpha H}$) values were determined from the high resolution DQF-COSY spectra by measuring the peak to peak distance on a cross-section parallel to the F_2 dimension where the digital resolution after zero filling was 0.5 Hz.

Hydrogen-deuterium exchange of the amide groups was studied using 65% ^2H_2O in aqueous solution and immediately recording the TOCSY spectrum and monitoring the NH-C$^\alpha$H cross-peaks in the fingerprint region. To determine the hydrogen-deuterium exchange of amide groups in methanol and $(CD_3)_2SO$, 20% CD_3OD and 15% ^2H_2O were used, respectively. The concentration of ^2H_2O in $(CD_3)_2SO$ was limited to 15% to avoid any complication that might arise due to conformational transition in these two solvents.

Variable temperature experiments have been recorded between 283 and 323 K (in methanol between 283 and 313 K), and the temperature was maintained by a Varian/Oxford temperature control unit with a sensitivity of ± 0.2 K. The NH chemical shifts varied linearly (high-field shift) with increasing temperature. The temperature coefficients ($d\delta/dT$) of amide chemical shifts were determined as the order of 10^{-3} ppm K^{-1}.

Restrained Molecular Modeling—Computer modeling of the molecular conformation of C16 was carried out using SYBYL molecular modeling software version 5.4 (Tripos Associates, Inc., St. Louis, MO) on an Evans & Sutherland PS390 computer. The program is set to generate all reasonably acceptable conformations of peptides that fit with the NMR parameters and NOE data. Because the peptide molecules appear to be largely populated in the α-helical conformations in $(CD_3)_2SO$, the NMR data in this solvent were used as restraints for molecular modeling. C16 was first built in an ideal α-helical conformation (ϕ, −57°, Ψ, −47°). It was then energy-minimized using high descents and used as the starting conformation for simulations. Both the NOE data and ϕ values deduced from $J_{NH\text{-}C^\alpha H}$ through Karplus equation (36) were used as constraints to generate a family of conformations of similar energy. The intensities of NOEs obtained at 250 ms mixing time were classified into strong, medium, and weak according to the number of contour levels (1–2, weak; 3–5, medium; >5, strong in a plot where the vertical intensity of each level is 1.4 times higher than that in the previous level), and distances of 4.8, 3.5, and 2.7, respectively, were used as the upper limit for the corresponding interproton distances (37, 38).

Circular Dichroism—CD spectra were recorded at 30 °C with a JASCO J-600 spectropolarimeter interfaced to an IBM PS/2 microcomputer. Measurements were carried out in cells with 0.1-cm path lengths using a peptide concentration of 0.3 mM. The peptide in aqueous DMPC dispersion was prepared by a similar method previously described (39), and the CD spectrum was recorded at 30 °C. The temperature control was achieved by circulating water through a cell jacket. DMPC (Sigma; 7.5 mM) was dissolved in chloroform and dried under a stream of nitrogen and then under vacuum. The peptide (0.4 mM) dissolved in sodium phosphate buffer (pH 7.4) was added, vortexed, and incubated at 30 °C (above the phase transition of the lipid) for 4 h. The lipid peptide molar ratio was 15:1. CD band intensities are expressed as molar ellipticities, $[\theta]_M$ in deg·cm^2·dmol^{-1}.

FTIR Measurements—Attenuated total reflectance Fourier transform infrared (ATR-FTIR) spectra in solution were recorded on a Bio-Rad FTS-40 spectrometer equipped with a deuterated triglycine sulfate detector and a Bio-Rad 3240-SPC computer for data acquisition and analysis. Spectra were recorded at 30 °C using a Micro Circle cell (Spectra-Tech, Inc., Stamford, CT) with a zinc selenide CIR (cylindrical internal reflectance) crystal in a stainless steel flow cell. A 1024-scan interferogram was collected at single beam mode with a resolution of 2 cm^{-1}, using a peptide concentration of 0.5 mM. The spectrometer was continuously purged with dry air to eliminate water vapor adsorptions. Solvent and sample spectra were recorded under identical conditions, and the difference spectra were obtained by digitally subtracting the solvent spectrum. The Bio-Rad Fourier manipulations software was used to obtain signal-enhanced deconvoluted spectra, using a half-bandwidth of 16 cm^{-1} and a K value of 2.3. The peptide dispersion in aqueous DMPC was prepared as described in the previous section with a lipid: peptide ratio of 15:1. The possibility of peptide adsorption on the zinc selenide crystal and the contribution of the adsorbed molecules in the ATR spectra were examined by carefully draining the peptide solution and replenishing with the media without disturbing the cell. The spec-

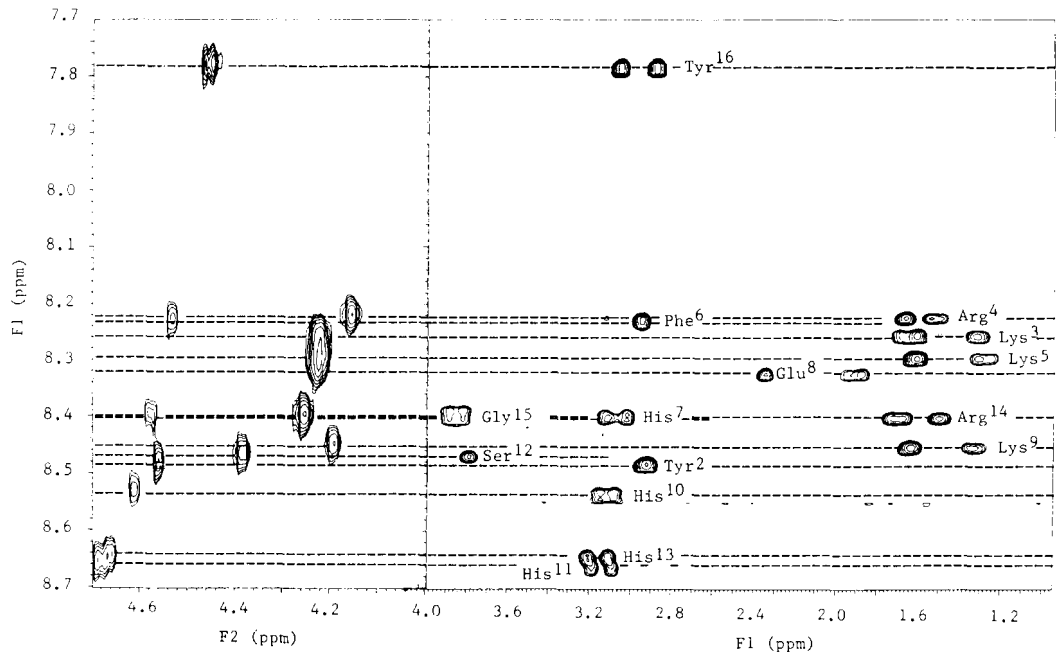

FIG. 2. **Part of the TOCSY spectrum of C16 showing the backbone amide resonance connectivities to $C^{\alpha}H$ and side-chain proton resonances.** The spectrum was recorded in $H_2O/^2H_2O$ at pH 3.8 and 30 °C.

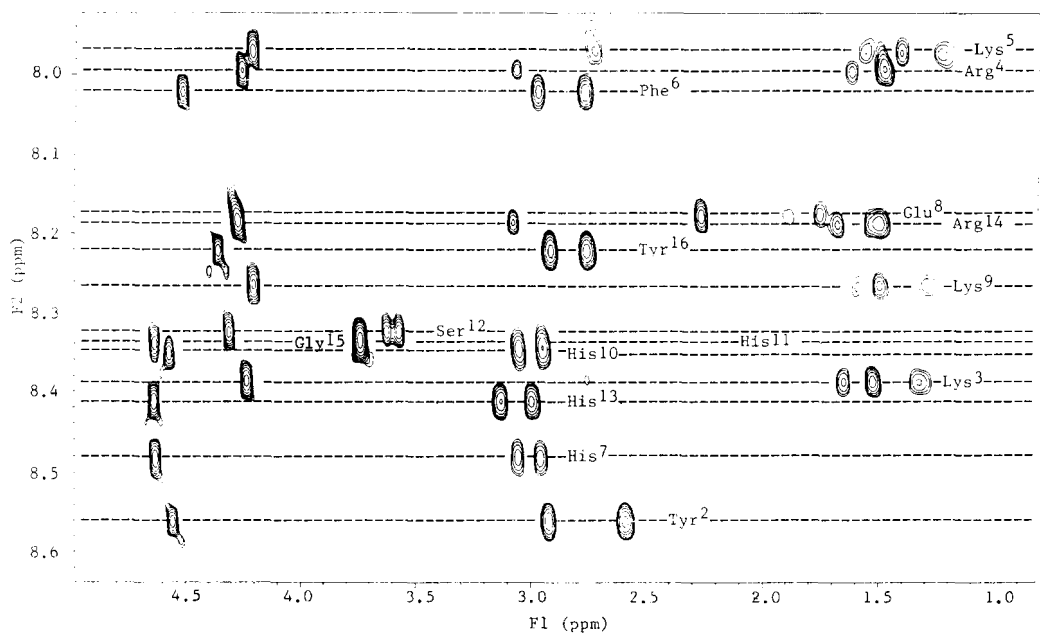

FIG. 3. **Part of the TOCSY spectrum of C16 showing backbone amide resonance connectivities to $C^{\alpha}H$ and side-chain proton resonances.** The spectrum was recorded in $(CD_3)_2SO$ at 30 °C.

tra recorded after draining and filling with the media did not show any significant absorption characteristic of the peptides, suggesting that peptide adsorption on the crystal is insignificant and that the ATR spectra are the mere reflection of the peptide molecules in solution.

RESULTS AND DISCUSSION

Sequential Resonance Assignments of C16—The resonance assignments of the ^1H NMR spectrum of the C16 fragment in water, CD_3OH and $(CD_3)_2SO$ were made by the standard sequential assignment procedures (35). The sequential resonance assignments in these three solvents were accomplished by the combined analyses of the 2D TOCSY and 2D NOE spectra. The 2D TOCSY spectra were also recorded at different temperatures (283–323 K) to resolve overlapping connectivities for unambiguous assignments. The 2D TOCSY spectra recorded at different temperatures have also been used to determine the temperature coefficients of NH chemical shifts. The backbone amide connectivities to the side-chain protons in the 2D TOCSY spectra in water and $(CD_3)_2SO$ are provided in Figs. 2 and 3. The unambiguous identification of most of the spin system was made from the amide protons relayed TOCSY connectivities (Figs. 2 and 3). Three lysine and two arginine residues were readily recognized by two distinct series of connectivities of their side chains to the backbone amide (Figs. 2 and 3) and side-chain amino protons. The Glu^8 and Ser^{12} residues were identified from their side-chain characteristic chemical shifts ($C^{\gamma}H$ at δ 2.2–0.5 ppm; $C^{\beta}H$ at δ 3.6–3.9 ppm, respectively) and their connectivities to the backbone amide protons. In addition, seven spin systems of three different protons whose $C^{\beta}H$ reso-

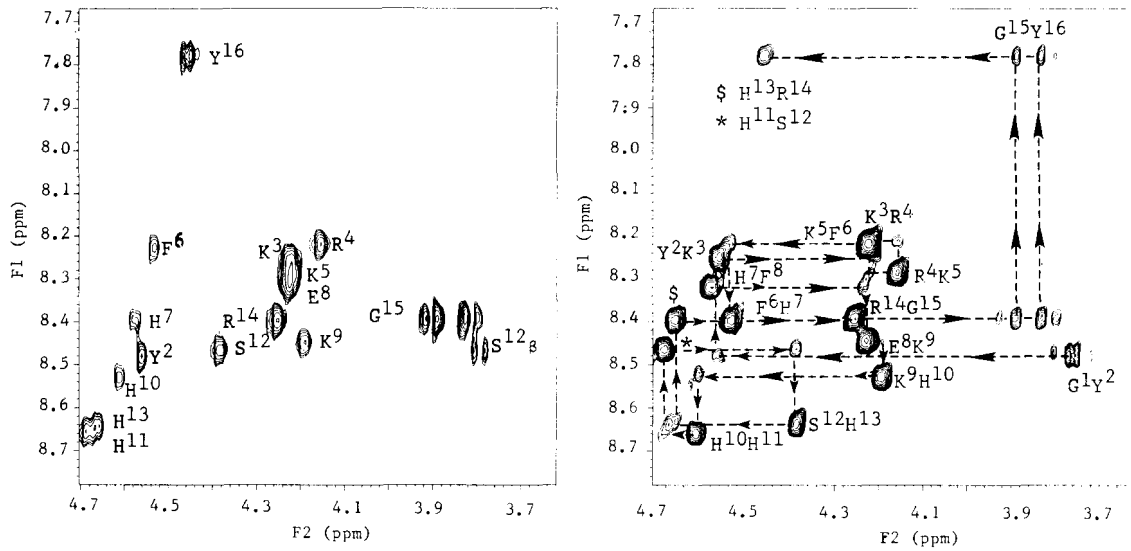

FIG. 4. **The fingerprint regions in the TOCSY (*left*) and NOESY (*right*) spectra of C16 in $H_2O/^2H_2O$ at pH 3.8 and 30 °C.** The αN connectivities in the TOCSY and αN (*i*, *i*+1) connectivities in the NOESY spectra are labeled.

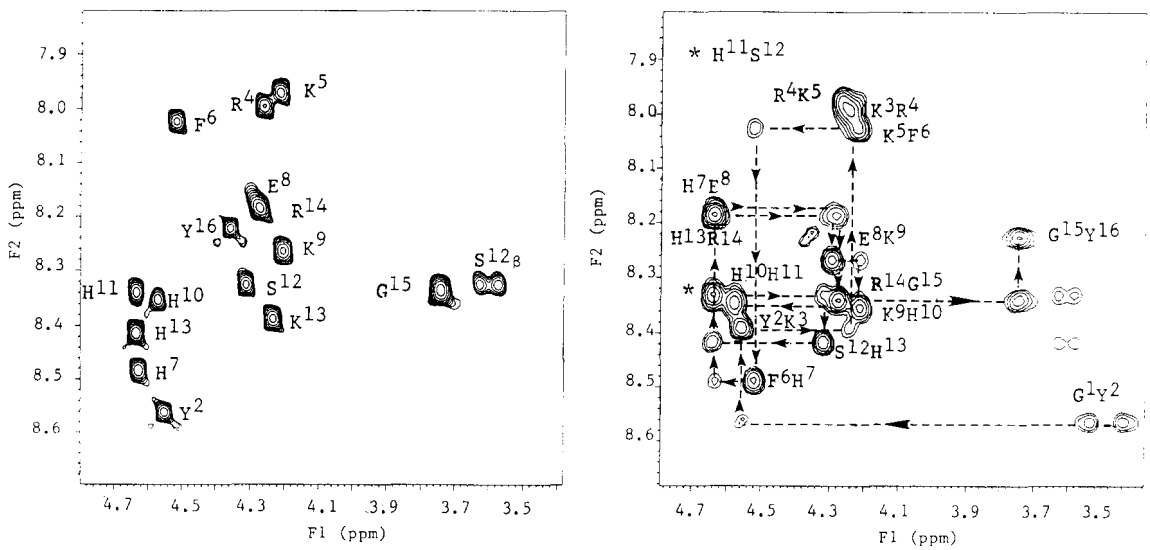

FIG. 5. **The fingerprint regions in the TOCSY (*left*) and NOESY (*right*) spectra of C16 in $(CD_3)_2SO$ at 30 °C.** The αN connectivities in the TOCSY and αN (*i*, *i*+1) connectivities in the NOESY spectra are labeled.

nances occur at δ 2.1–3.3 ppm corresponding to four His, two Tyr, and Phe[6] residues were also identified in the TOCSY spectra.

The assignment of resonances to individual amino acids was accomplished by the combined analyses of the NH-C$^{\alpha}$H connectivities in the fingerprint regions in the TOCSY and 2D NOE spectra. The fingerprint regions of the TOCSY and NOESY spectra in aqueous and $(CD_3)_2SO$ solutions are provided in Figs. 4 and 5. Both the fingerprint regions in the TOCSY and NOESY spectra are well dispersed, and sequential assignments of the resonances were unambiguously determined on the basis of αN (*i*, *i*) and αN (*i*, *i*+1) connectivities. The αN connectivity of Gly[1]-Tyr[2] was a convenient starting point. Each sequential dipeptide connectivity was further confirmed by the βN connectivity, which suggested the identity of the amino acid residue. The NOE connectivities between the aromatic ring and the αβ protons have been used to assign the respective ring protons to individual residues. The protons of the N-terminal amino group, C-terminal carboxyl group, and hydroxyl groups of Ser[12], Tyr[2], and Tyr[16] were not identified presumably due to their fast exchange with the solvent protons.

The chemical shifts of all of the assigned protons in water, $(CD_3)_2SO$, and CD_3OH are listed in Tables I, II, and III, respectively. The temperature coefficients of NH chemical shifts and coupling constants ($J_{NH\text{-}C^{\alpha}H}$) are provided in Table IV. The NH-C$^{\alpha}$H region of the DQF-COSY spectrum in CD_3OH and the NH-NH region of the NOESY spectrum in $(CD_3)_2SO$ are provided in Fig. 6. The summary of the observed NOE connectivities are provided in Fig. 7.

Conformational Analysis in Aqueous Solution—The summary of NMR and NOE parameters are provided in Table IV and Fig. 7, respectively. A set of characteristic strong, medium, and weak NOE connectivities, $J_{NH\text{-}C^{\alpha}H}$ values, temperature coefficients of NH chemical shifts, and fast $^1H/^2H$ exchange of amide groups have been considered as criteria to examine whether the C16 linear sequence has any preferred backbone conformation in aqueous solution. The temperature coefficients of all amide resonances provided in Table IV are high (≥0.0041 ppm K^{-1}) suggesting that the backbone NH groups are exposed to the solvent and not involved in any intramolecular hydrogen-bonding interactions. In 65% ^2H_2O, the amide groups of all residues except Lys[9], Arg[14], and Tyr[16] got exchanged in 10 min.

TABLE I

^1H chemical shifts (parts/million) of the active C-terminal fragment (C16) of salivary histatin 5 in H_2O/D_2O at 30 °C, pH 3.8

Chemical shifts were determined ±0.02 ppm relative to the proton resonance of H_2O or HOD at 4.7 ppm.

Residue	NH	$C^{\alpha}H$	$C^{\beta}H$	$C^{\gamma}H$	Others
Gly^1		3.82, 3.77			
Tyr^2	8.48	4.56	2.93		$C^{\delta}H$ 7.01; $C^{\epsilon}H$ 6.63
Lys^3	8.24	4.23	1.72	1.32	$C^{\delta}H$ 1.62; $C^{\epsilon}H$ 2.73; $N^{\epsilon}H_2$ 7.65
Arg^4	8.22	4.15	1.73	1.60, 1.54	$C^{\delta}H$ 3.27; $N^{\delta}H_2$ 7.58
Lys^5	8.30	4.23	1.61	1.32, 1.23	$C^{\delta}H$ 1.64; $C^{\epsilon}H$ 2.70; $N^{\epsilon}H_2$ 7.17
Phe^6	8.23	4.55	2.96		$C^{\delta}H$ 7.21; $C^{\epsilon}H$ 7.33; $C^{\zeta}H$ 7.44
His^7	8.40	4.57	3.16, 3.07		C^2H 8.01; C^4H 7.21
Glu^8	8.33	4.23	1.96, 1.85	2.32	
Lys^9	8.45	4.19	1.64	1.32	$C^{\delta}H$ 1.59; $C^{\epsilon}H$ 2.76; $N^{\epsilon}H_2$ 7.01
His^{10}	8.53	4.61	3.12, 3.06		C^2H 8.02; C^4H 7.31
His^{11}	8.66	4.69	3.20, 3.09		C^2H 8.15; C^4H 7.23
Ser^{12}	8.46	4.38	3.80		
His^{13}	8.45	4.67	3.22, 3.12		C^2H 8.08; C^4H 7.28
Arg^{14}	8.39	4.25	1.72	1.48	$C^{\delta}H$ 2.97; $N^{\delta}H_2$ 7.05
Gly^{15}	8.39	3.91, 3.82			
Tyr^{16}	7.79	4.46	3.04, 2.85		$C^{\delta}H$ 7.67; $C^{\epsilon}H$ 6.62

TABLE II

^1H chemical shifts (parts/million) of the active C-terminal fragment (C16) of salivary histatin 5 in $(CD_3)_2SO$ at 30 °C

Chemical shifts were determined ±0.02 ppm relative to tetramethylsilane.

Residue	NH	$C^{\alpha}H$	$C^{\beta}H$	$C^{\gamma}H$	Others
Gly^1		3.55, 3.42			
Tyr^2	8.57	4.56	2.93, 2.59		$C^{\delta}H$ 7.03; $C^{\epsilon}H$ 6.65
Lys^3	8.39	4.25	1.66	1.33	$C^{\delta}H$ 1.53; $C^{\epsilon}H$ 2.75; $N^{\epsilon}H_2$ 7.85
Arg^4	7.99	4.26	1.68	1.50	$C^{\delta}H$ 3.08; $N^{\delta}H_2$ 7.73
Lys^5	7.97	4.22	1.56	1.24	$C^{\delta}H$ 1.49; $C^{\epsilon}H$ 2.73; $N^{\epsilon}H_2$ 7.87
Phe^6	8.02	4.53	2.98, 2.78		$C^{\delta}H$ 7.23; $C^{\epsilon}H$ 7.35; $C^{\zeta}H$ 7.46
His^7	8.48	4.64	3.05, 2.96		C^2H 8.03; C^4H 7.23
Glu^8	8.17	4.25	2.28	1.89, 1.69	
Lys^9	8.27	4.21	1.60	1.29	$C^{\delta}H$ 1.51; $C^{\epsilon}H$ 2.77; $N^{\epsilon}H_2$ 7.83
His^{10}	8.35	4.57	3.05, 2.96		C^2H 8.12; C^4H 7.33
His^{11}	8.34	4.63	3.05, 2.96		C^2H 8.17; C^4H 7.21
Ser^{12}	8.33	4.31	3.64, 3.58		
His^{13}	8.41	4.64	3.13, 3.00		C^2H 8.12; C^4H 7.32
Arg^{14}	8.18	4.27	1.68	1.50	$C^{\delta}H$ 3.03; $N^{\delta}H_2$ 7.68
Gly^{15}	8.34	3.78, 3.73			
Tyr^{16}	8.22	4.35	2.93, 2.76		$C^{\delta}H$ 7.69; $C^{\epsilon}H$ 6.64

TABLE III

^1H chemical shifts (parts/million) of the active C-terminal fragment (C16) of salivary histatin 5 in CD_3OH at 30 °C

Chemical shifts were determined ±0.02 ppm relative to tetramethylsilane.

Residue	NH	$C^{\alpha}H$	$C^{\beta}H$	$C^{\gamma}H$	Others
Gly^1		3.83, 3.74			
Tyr^2	8.85	4.34	3.03, 2.95		$C^{\delta}H$ 7.04; $C^{\epsilon}H$ 6.71
Lys^3	8.50	4.06	1.84	1.35, 1.49	$C^{\delta}H$ 1.66; $C^{\epsilon}H$ 2.92; $N^{\epsilon}H_2$ 7.50
Arg^4	8.15	4.14	1.85, 1.70	1.57	$C^{\delta}H$ 3.18; $N^{\delta}H_2$ 7.58
Lys^5	8.00	4.07	1.79	1.38, 1.48	$C^{\delta}H$ 1.63; $C^{\epsilon}H$ 2.96; $N^{\epsilon}H_2$ 7.50
Phe^6	8.30	4.23	3.14, 3.00		$C^{\delta}H$ 7.21; $C^{\epsilon}H$ 7.32; $C^{\zeta}H$ 7.44
His^7	8.31	4.45	3.31, 3.14		C^2H 8.01; C^4H 7.21
Glu^8	8.42	4.13	2.13	2.54, 2.42	
Lys^9	8.14	4.09	1.87, 1.78	1.35, 1.46	$C^{\delta}H$ 1.58; $C^{\epsilon}H$ 3.12; $N^{\epsilon}H_2$ 7.62
His^{10}	7.95	4.47	3.13, 2.89		C^2H 8.18; C^4H 7.31
His^{11}	8.16	4.56	3.25, 3.12		C^2H 8.20; C^4H 7.25
Ser^{12}	8.19	4.31	3.89, 3.81		
His^{13}	8.32	4.62	3.31, 3.35		C^2H 8.09; C^4H 7.34
Arg^{14}	8.16	4.29	1.85, 1.71	1.57	$C^{\delta}H$ 3.12; $N^{\delta}H_2$ 7.32
Gly^{15}	8.29	3.94, 3.78			
Tyr^{16}	7.79	4.43	3.06, 2.90		$C^{\delta}H$ 7.01; $C^{\epsilon}H$ 6.66

The other three NH groups were also exchanged after 2 h. The fast $^1H/^2H$ exchange rate observed for all backbone amide resonances (Table IV) in 65% ^2H_2O provides further evidence that the amide groups are not involved in any intramolecular hydrogen bonding in aqueous solution. The prevalence of strong $\alpha N\ (i, i+1)$ and weak $\alpha N\ (i, i)$ NOEs (Fig. 4) with a continuous stretch of weak and medium $\beta N\ (i, i)$ and $\alpha\beta\ (i, i)$ (Fig. 7) in the absence of any observable NN NOE interactions suggests that the backbone dihedral angles are predominantly in the unfolded, extended region of ϕ, ψ space (35, 40). The $J_{NH\text{-}C}\alpha_H$ values provided in Table IV are ≥7.4 Hz for all residues except Gly^{15}. For a regular β-strand, the $J_{NH\text{-}C}\alpha_H$ is expected to be ~9 Hz (35, 40, 41). The coupling constants of 7.4–8.5 Hz observed for this linear flexible peptide suggest the populations of unfolded nonhydrogen-bonded conformations of comparable energy with ϕ values exceeding the regular helical region. Collectively, the NMR parameters in water provide evidence that the conformational ensemble of the peptide molecules includes only unfolded random structures.

Conformational Analysis in Organic Solutions—In $(CD_3)_2SO$

and CD_3OH, lowered temperature coefficients of backbone amide groups ($\leq$0.0027) except Tyr^2, Lys^3, and Arg^4 have been observed (Table IV) indicating that 12 amide NH groups from Lys^5 to Tyr^{16} are partially solvent-shielded. This indicates that these amide NH groups may presumably be involved in intramolecular hydrogen bonding, whereas the three NH groups of Tyr^2, Lys^3, and Arg^4 are well exposed to the solvent. The observation of such lowered $d\delta/dT$ ($\leq$0.003 ppm K^{-1}) has generally been attributed to intramolecularly hydrogen-bonded amide groups in linear peptides (42–47). However, in CD_3OH, the Arg^4 NH group exhibits an intermediate $d\delta/dT$ value (0.0032 ppm K^{-1}). In acyclic peptides, such moderate temperature coefficients are difficult to interpret, although they have been frequently assigned to weakly hydrogen-bonded amide groups (46, 48–50). An intermediate $d\delta/dT$ value could also arise due to population of conformations with and without the involvement of Arg^4 in intramolecular hydrogen bonding. The slow $^1H/^2H$ exchange of the Lys^5 to Tyr^{16} NH groups (Table IV) also suggests that they may be inaccessible to the solvent and presumably intramolecularly hydrogen-bonded (51, 52). In these two organic solutions, the $J_{NH\text{-}C}\alpha_H$ values fall in the range of 5.0–6.5 Hz for all residues except the C-terminal Tyr^{16} (Table IV). The $J_{NH\text{-}C}\alpha_H$ values expected for an ideal α-helix (ϕ, −57°) and 3_{10}-helices (ϕ, −60°) are of the order of 3.9 and 4.2 Hz, respectively. However, in flexible linear peptides, even for quite large helical populations, $J_{NH\text{-}C}\alpha_H$ values have been expected to be ~6–7 Hz (40). In addition, over 80% of protein helical segments with 3–5 subsequent residues have $J_{NH\text{-}C}\alpha_H$ values of ~6 Hz (35). Therefore, it is reasonable to assume that the $J_{NH\text{-}C}\alpha_H$ values (5.0–6.5 Hz) observed for most residues of C16 indicate that the populations of conformations in both CD_3OH and $(CD_3)_2SO$ have ϕ values (ϕ, −57 ± 20°) that fall in the helical region.

TABLE IV
^{1}HNMR parameters for the active fragment (C16) of salivary histatin 5

$J_{NH\text{-}C^{\alpha}H}$ values were determined from 2D DQF-COSY spectra with a digital resolution of ±0.5 Hz.

Residue	H_2O/D_2O		CD_3OH		$(CD_3)_2SO$	
	$J_{NH\text{-}C^{\alpha}H}$	$d\delta/dT$	$J_{NH\text{-}C^{\alpha}H}$	$d\delta/dT$	$J_{NH\text{-}C^{\alpha}H}$	$d\delta/dT$
	Hz	*ppm K^{-1} × 10^3*	*Hz*	*ppm K^{-1} × 10^3*	*Hz*	*ppm K^{-1} × 10^3*
Gly^1						
Tyr^2	8.5	5.8	6.5	5.4	6.2	5.8
Lys^3	7.8	5.4	6.0	4.8	6.1	4.9
Arg^4	7.4	5.2	6.3	3.2	5.4	4.0
Lys^5	8.4	4.8	7.0	2.6	6.8	2.4
Phe^6	8.1	4.6	6.8	2.4	7.0	2.6
His^7	7.9	4.1	5.0	2.6	5.5	2.2
Glu^8	7.5	4.2	6.2	2.2	5.8	2.3
Lys^9	7.7	4.8	5.7	2.5	6.0	2.5
His^{10}	7.9	4.2	5.5	2.2	6.2	2.2
His^{11}	8.0	4.4	5.7	2.4	6.0	2.1
Ser^{12}	7.4	4.6	5.8	2.2	5.4	2.5
His^{13}	8.0	4.2	5.5	2.3	5.8	2.2
Arg^{14}	7.8	4.5	6.5	2.7	6.2	2.5
Gly^{15}	6.8, 6.6	4.3	5.3, 5.2	2.6	5.4, 5.6	2.4
Tyr^{16}	7.9	4.6	7.1	2.8	6.6	2.6

The summary of sequential and medium range NOEs observed for C16 in CD_3OH and $(CD_3)_2SO$ (Figs. 6, *right*, and 7) shows sequential NN (i, i+1) and medium range α (i, i+3) interactions, characteristic of α-helical conformations (35, 37, 40). However, only a few of the complete set of weak NOEs such as αN (i, i+2) and αN (i, i+3) expected for ideal α- and 3_{10}-helical conformations are observed. Because the measured NOE intensities reflect a population-weighted average over all conformations in solutions (40), the absence of some weak NOEs may be due to fluctuation over an ensemble of conformations with a range of ϕ and ψ angles lying within the helical space. In addition, the expected long range NOEs follow the assumption that the structures are rigid and that the same correlation function, $f(\tau_c)$ applies for all connectivities (35). Nevertheless, the observation of strong and medium NN (i, i+1), $\alpha\beta$ (i, i+3) NOEs provides convincing evidence for the prevalence of at least a threshold population of α-helical conformations. Collectively, the above data indicate that C16 displays significant populations of α-helical conformers, which are stabilized by 12 (5 • 1) intramolecular hydrogen bonds in CD_3OH and $(CD_3)_2SO$.

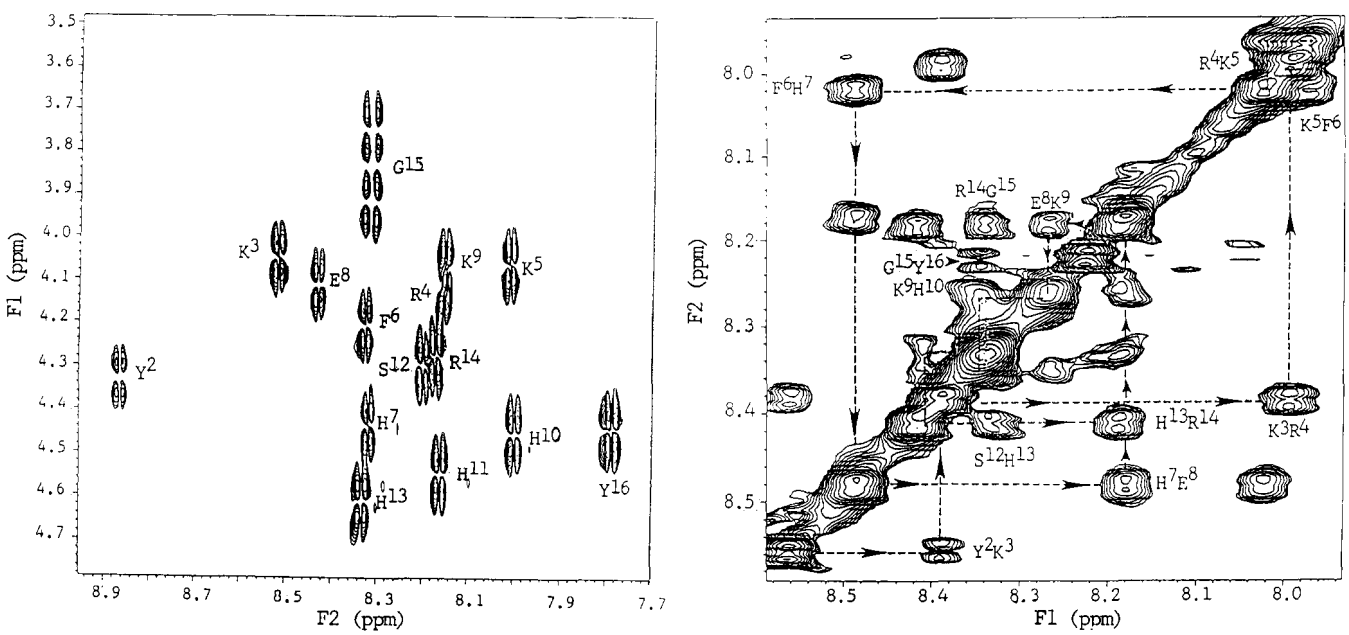

FIG. 6. Part of the DQF-COSY spectrum (*left*) of C16 illustrating $J_{NH\text{-}C\alpha H}$ coupling connectivities, in CD_3OH at 30 °C. Both positive and negative contours are plotted. Partial NOESY spectrum (*right*) illustrating the NN (i, i+1) connectivities in $(CD_3)_2SO$ at 30 °C. Only the well resolved contours are labeled. The N-N connectivities of His^{10}-His^{11} and His^{11}-Ser^{12} are not well resolved due to close proximity of their chemical shifts (δ 8.33–8.35 ppm).

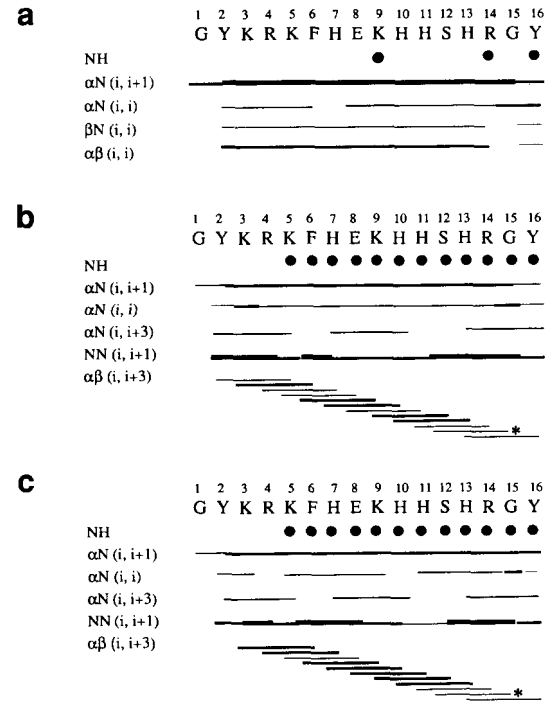

FIG. 7. **Summary of sequential and medium range NOE data compiled from the NOESY spectra of C16 recorded at 30 °C in (*a*) $H_2O/^2H_2O$, (*b*) CD_3OH, and (*c*) $(CD_3)_2SO$ using the mixing time of 150, 300, and 250 ms, respectively.** The thickness of the *bars* indicates the NOE is strong, medium, and weak, respectively. The * marked NOEs are between $C^{\alpha}H$ of Ser^{12} and one of the $C^{\alpha}H$ of Gly^{15}.

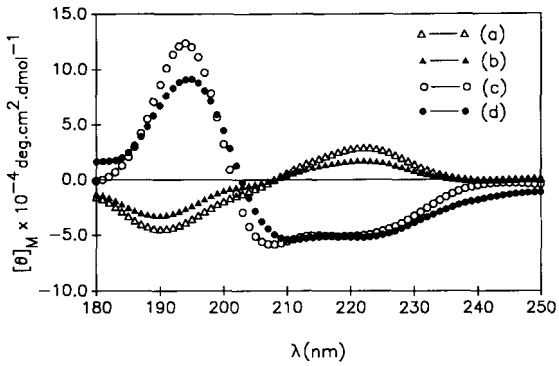

FIG. 8. **The CD spectra of C16 recorded at 30 °C in (*a*) water at pH 3.8, (*b*) sodium phosphate buffer at pH 8.3, (*c*) TMP, and (*d*) DMPC vesicles (peptide:lipid molar ratio 1:15).**

The possibility of the presence of minor populations of 3_{10}-helical conformations in the two organic solvents has also been examined. The α- (ϕ, −57 ± 20°; ψ, −47 ± 20°) and 3_{10}- (−60 ± 20°; ψ, −30 ± 20°) helical conformations differ essentially in the intramolecular hydrogen-bonding pattern, *viz.* 5 → 1 and 4 → 1, respectively. The moderately low temperature coefficient (0.0032 ppm K^{-1}) observed for Arg^4 in CD_3OH (Table IV) suggests that this amide group could also be involved in a weak intramolecular interaction and that considerable 3_{10}-helical populations could be present together with the major α-helical conformations. The differences in the amide NH and $C^{\alpha}H$ chemical shifts and the intensity of medium range αβ (*i*, *i*+3) NOEs in CD_3OH and $(CD_3)_2SO$ most probably reflect the relative populations of α- and 3_{10}-helical conformations. Thus, NMR evidence suggests that C16 exists mostly as α-helical conformations with minor populations of 3_{10}-conformers in methanolic solution, whereas α-helical conformers predominate in $(CD_3)_2SO$.

TABLE V
CD parameters for the active C-terminal fragment (C16) of salivary histatin 5

Peptide concentration, 0.3 mM.

Solvent[a]	λ	$[\theta]_M \times 10^{-4}$	λ	$[\theta]_M \times 10^{-4}$	λ	$[\theta]_M \times 10^{-4}$
	nm		*nm*		*nm*	
Water (pH, 3.8)	190	−4.54			222	+2.86
Phosphate buffer[b] (pH, 7.4)	192	−9.24			218	+1.70
Phosphate buffer (pH, 8.3)	190	−3.2			222	+1.71
TMP	194	+12.38	208	−5.85	217	−5.12
DMPC	194	+9.16	211	−5.44	221	−5.23

[a] $[\theta]_M$ expressed as deg·cm²·dmol⁻¹.
[b] Values from Raj *et al.* (23).

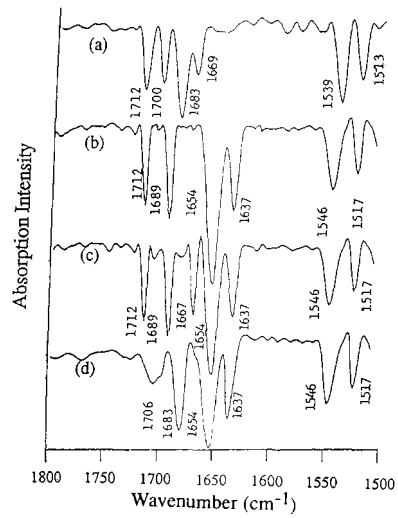

FIG. 9. **Deconvoluted ATR-FTIR absorption spectra from 1800–1500 cm^{-1} of C16 in (*a*) sodium phosphate buffer at pH 7.4, (*b*) dimethyl sulfoxide, (*c*) methanol, and (*d*) DMPC vesicles (peptide:lipid molar ratio 1:15).**

CD Studies—CD studies of C16 were performed to compare findings obtained with NMR and to delineate the effect of lipid interaction on the conformation of the histatin peptide. The CD spectra recorded between 180–250 nm in water (pH 3.8) and sodium phosphate buffer (pH 8.3), TMP and in DMPC vesicles are provided in Fig. 8, and the CD parameters are summarized in Table V. Because dimethyl sulfoxide is not transparent to the CD region (180–235 nm), a comparable polar and aprotic solvent TMP was used to compare the NMR results in $(CD_3)_2SO$. The CD spectrum of C16 in water at pH 3.8 exhibits a weak positive band at ~222 nm ($[\theta]_M$, 2.86×10^4 deg·cm²·dmol⁻¹) and a fairly strong negative band ($[\theta]_M$, -4.54×10^4 deg·cm²·dmol⁻¹) at ~190 nm (Fig. 8 and Table V). The CD spectrum of C16 in phosphate buffer at pH 8.3 was not significantly different from the spectrum in water at pH 3.8 (Fig. 8). The previously reported CD spectrum of C16 in aqueous sodium phosphate buffer at pH 7.4 also exhibited a weak positive band at ~220 nm and a strong negative band at 190 nm (23), resembling the spectrum of unordered random conformation (53). The results suggest that the conformation of C16 is unordered in aqueous solutions over the pH range 3.8–8.3 and is consistent with the NMR data.

In TMP, C16 showed two negative bands at ~217 nm ($[\theta]_M$, -5.12×10^4 deg·cm²·dmol⁻¹) and ~208 nm ($[\theta]_M$, -5.85×10^4 deg·cm²·dmol⁻¹) and a positive maximum at ~194 nm (Fig. 8 and Table V). The spectrum is reminiscent of the CD spectra of helical polypeptides (53–58). The two negative bands at 208 and 217 nm observed for C16 correspond to the long wavelength component of exciton split of the π-π^* and the n-π^* transitions, respectively. The CD spectrum of the peptide in

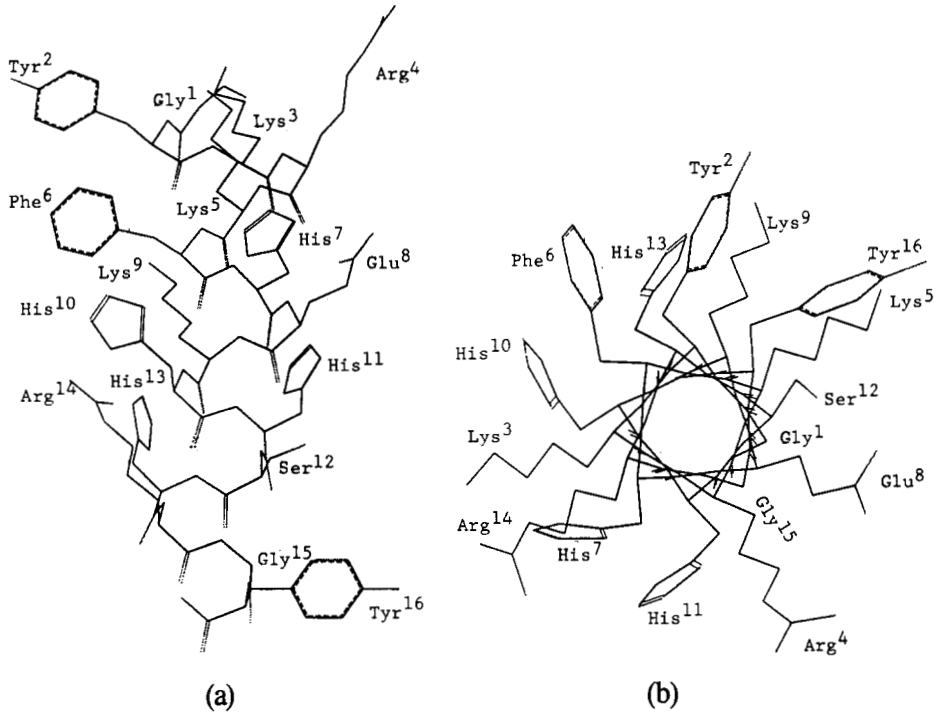

FIG. 10. *a*, perspective view of the α-helical backbone of C16 deduced from molecular modeling using the NMR and NOE data in $(CD3)_2SO$ as constraints. *b*, a view of the helical conformation of C16 through the helix axis showing a relatively weak amphipathic nature of the peptide with His^{10}, Phe^6, His^{13}, Tyr^2, Lys^9, and Tyr^{16} on the apolar face of the helix.

DMPC vesicles also resembles those of helical polypeptides exhibiting two negative bands at ~221 ($[\theta]_M$, -5.23×10^4 deg·cm^2·dmol^{-1}) and ~211 nm ($[\theta]_M$, -5.44×10^4 deg·cm^2·dmol^{-1}) with a positive band at ~194 nm (Fig. 8 and Table V). Similar CD band shapes have been generally ascribed to α-helical structures (53, 54). The CD spectra in TMP and DMPC are also reminiscent of the previously reported CD spectrum of this peptide in methanol (23). The CD data suggest that polar organic solvents and a lipid environment induce the peptide to fold into helical conformations. The diminished CD band intensity observed for this peptide could be due to the short chain length of this peptide. Indeed, the influence of peptide chain length on the CD band intensities has been observed for helical peptides, and lowered ellipticity values have been attributed to the shorter chain length of peptides (58, 59). The shortening of helix by end-fraying and by deviation of the backbone dihedral angles from the ideal values has also been reported to affect the CD band intensities (40). Nevertheless, the CD spectra of C16 in TMP and DMPC provide evidence that in polar organic solvents and in lipid vesicles, helical conformations are significantly populated. However, the CD spectra of α- and 3_{10}-helical peptides are very similar, and chiroptical distinctions between these conformations cannot be made from CD data alone (57). Recently, FTIR studies have been used to distinguish α- and 3_{10}-conformations using amide I frequencies of peptides in solution (60).

FTIR Studies—ATR-FTIR was used to obtain signal enhancement of the spectrum in solution, handle aqueous solutions without compensating for very strong solvent absorptions, and eliminate the complications of using high peptide concentrations and deuterated solvents (61, 62). The micro circle cell equipped with a zinc selenide cylindrical internal reflectance (CIR) crystal has been shown to overcome the strong infrared absorption by water, because the infrared penetrates a relatively short distance regardless of its thickness. The short and reproducible pathlength inherent in the CIR crystal cell allows accurate subtraction of background solvent bands as compared with conventional transmission cells (63, 64). We used the CIR technique to examine the conformational features of the linear peptide in aqueous and organic solutions. The amide I and amide II regions of the deconvoluted ATR-FTIR spectra of C16 in sodium phosphate buffer (pH 7.4), dimethyl sulfoxide, methanol, and DMPC are provided in Fig. 9. In aqueous buffer, the amide I absorption consists of four components at 1669, 1683, 1700, and 1712 cm^{-1}, and the amide II absorption has two components at 1539 and 1513 cm^{-1} (Fig. 9). The band identified at 1712 cm^{-1} could be related to the carbonyl group of carboxyl functions, whereas the strong bands at 1700 and 1683 cm^{-1} could be free carbonyls of the peptide bonds. These bands suggest that nonhydrogen-bonded conformations are significantly populated in aqueous buffer solutions. The absence of strong bands between 1653 and 1667 cm^{-1} suggests that helical conformations are not favored in aqueous solutions. The weak band at 1669 cm^{-1} could be the contribution from a minor population of scattered turn conformations. In dimethyl sulfoxide, the amide I region has bands at 1637, 1654, 1689, and 1712 cm^{-1} (Fig. 9). The band at 1712 and 1689 cm^{-1} may be attributed to free carbonyls of the carboxyl and amide functions, respectively. The strong band at 1654 cm^{-1} and the amide II components at 1546 and 1517 cm^{-1} suggest that α-helical conformations are significantly populated in dimethyl sulfoxide solutions. The amide I at 1654 cm^{-1} and amide II bands at 1546 and 1517 cm^{-1} are consistent with those observed for α-helical polypeptides (65). The band at 1637 cm^{-1} may arise from the $3\pi/2$ vibration of α-helix. The weak vibrational amide I components at 1639 and 1648 cm^{-1} observed for linear helical peptides have been assigned to type III β-turn with a possible contribution from the $3\pi/2$ vibration of α-helix (60). The amide I band that occurs between 1652–1659 cm^{-1} has been assigned to α-helix in linear peptides (60). In the methanolic solution, the peptide exhibits amide I components at 1712, 1689, 1667, 1654, and 1637 cm^{-1} and amide II bands at 1546 and 1517 cm^{-1} (Fig. 9). The bands at 1712 and 1689 cm^{-1} represent the free carbonyls of the carboxyl functions and amide functions, respectively. The strong amide I band at 1654 cm^{-1} and the relatively weak band at 1667 cm^{-1} could be assigned to α-helical and 3_{10}-helical conformations, respectively. The occurrence of bands at 1654 and 1667 cm^{-1} in the amide I

region has recently been attributed to the presence of mixed populations of α-helical and 310-helical conformations in solutions of linear peptides (60). In DMPC vesicles, the amide I bands have components at 1637, 1654, 1683, and 1706 cm^{-1}, whereas amide II bands occur at 1546 and 1517 cm^{-1} (Fig. 9). The bands at 1683 cm^{-1} and 1706 cm^{-1} (Fig. 9) are assigned to free carbonyls of peptide and carboxyl groups, respectively. The strong amide I band at 1654 cm^{-1} and the amide II bands at 1546 and 1517 cm^{-1} could be assigned to an α-helix.

The FTIR data suggest that the peptide prefers random non-hydrogen-bonded structures in aqueous buffer solutions. In dimethyl sulfoxide and DMPC vesicles, the amide I band at 1654 cm^{-1} provides evidence for the presence of α-helical conformations. The presence of amide I components at 1654 cm^{-1} and at 1667 cm^{-1} indicates the mixed populations of α- and 3_{10}-helical conformations in methanolic solutions.

Conformation and Biological Activity—The physiological activities of antimicrobial peptides are generally ascribed to their effects on membranes (66). Hence, the structure-function relationships of these peptides have been explained by the conformations they adopt in membranes rather than in aqueous medium (67, 68). The candidacidal activity of histatins has been shown to involve membrane interaction and alteration of ionic gradient across membranes (2, 9, 13). The loss of viability has been found to be concomitant with the loss of potassium from yeast cells exposed to salivary histatins (2, 9). Salivary histatins have recently been reported to lyse cells of *C. albicans* (69). These observations provide convincing evidence that the cidal activity of histatins is the consequence of their interaction with cell membranes. The conformational transition observed for this histatin sequence in aqueous solution and DMPC vesicles suggests that the randomly populated peptide molecules in the aqueous phase could interact initially with the lipid phase of membranes and take ordered helical conformations, which facilitate the binding of the charged and polar residues with the polar face of the membranes. A restrained α-helical model has been generated for C16 using molecular modeling techniques and the NMR data in $(CD_3)_2SO$ (see "Experimental Procedures"), which mimics the polar aprotic membrane environment. The lower ϕ values deduced from $J_{NH\text{-}C}\alpha_H$ and the NOE distances were essentially used as constraints to generate a family of closely related structures that have very similar energy and average backbone atomic positions. An average of 15 such structures consistent with the NMR data is provided in Fig. 10. The backbone conformational angles of the α-helical model shown in Fig. 10*a* deviate ± 20° from the ideal ϕ and ψ values except for Lys^5 and Tyr^2. The structural features suggest that the peptide could bind to the polar face of membranes interacting with the head groups, which are virtually aligned parallel to the plane of the lipid bilayer.

Most antimicrobial cationic polypeptides have been reported to form either α-helical or β-sheet structures exhibiting amphiphilic character (24–27). The spontaneous insertion of these amphiphilic peptides into cell membranes and formation of ion channels have been suggested as the probable mechanism of their cidal action (24, 26). The amphiphilicity of the helical conformation of C16 and the possibility of its insertion into membranes have been examined. The Lys and Arg residues of C16 are expected to be charged at physiological pH. Moreover, all other residues are polar except the two Gly residues at positions 1 and 15. The helical wheel diagram shown in Fig. 10*b* suggests only a relatively weak amphipathic character with a single hydrophobic residue (Phe^6) and the partial hydrophobicity offered by His^{10}, His^{13}, Tyr^2, and Tyr^{16} residues on the apolar face of the helix. The spontaneous insertion of the peptide into the hydrophobic barrier of membranes appears unlikely as the helical structure (Fig. 10*b*) lacks sufficient amphipathic character. Overall, the peptide appears quite polar and hydrophilic suggesting that the mechanism of cidal action of this peptide may, indeed, be different from that of other cationic antimicrobial peptides such as magainins, defensins, tachyplesins, and polyphemucins, which can spontaneously insert into membranes with their amphiphilic structures (26). The polar and hydrophilic nature of C16 and other histatins suggest that their binding to cell membranes could involve primarily electrostatic and hydrogen-bonding interactions, which then favor its migration within the membrane. It is pertinent to mention that electrostatic binding of positively charged residues of membrane proteins with the head groups of the acidic lipids has recently been reported (70). The positively charged residues at the N- and C-terminal regions of C16 could bind electrostatically to the head groups of the acidic lipids, while the polar residues could interact by forming hydrogen bonds. The membrane-bound peptide may then disrupt membrane structure and cause impairment of influx and efflux of the target cells leading to cell damage.

In summary, the spectroscopic analyses of C16 suggest that the candidacidal domain of salivary histatin 5 is structurally flexible and undergoes solvent-dependent conformational transition. In dimethyl sulfoxide and DMPC vesicles, which mimic the polar aprotic nature of membranes, C16 prefers to adopt helical conformation suggesting that the peptide could bind to membranes with its helical conformation. The weak amphipathic character of the helical structure seems to exclude the possibility of spontaneous insertion of the peptide into membranes. Electrostatic and hydrogen-bonding interactions of histatins with the polar head groups of plasma membranes of target cells appear to be the possible initial step involved in the mechanism of their antimicrobial activity.

REFERENCES

1. Minaguchi, K., and Bennick, A. (1989) *J. Dent. Res.* **68,** 2–15
2. Oppenheim, F. G. (1989) in *Human Saliva: Clinical Chemistry and Microbiology* (Tenovuo, J. O., ed) CRC Press, Boca Raton, Florida
3. Troxler, R. F., Offner, G. D., Xu, T., vanderSpek, J. C., and Oppenheim, F. G. (1990) *J. Dent. Res.* **69,** 2–6
4. Hay, D. I. (1975) *Arch. Oral Biol.* **20,** 553–558
5. Oppenheim, F. G., Yang, Y. C., Diamond, R. D., Hyslop, D., Offner, G. D., and Troxler, R. F. (1986) *J. Biol. Chem.* **261,** 1177–1182
6. Richardson, C. F., Johnsson, M., Raj, P. A., Levine, M. J., and Nancollas, G. H. (1993) *Arch. Oral Biol.* **38,** 997–1002
7. Holbrook, I. B., and Molan, P. C. (1975) *Biochem. J.* **149,** 489–492
8. MacKay, B. J., Denepitiya, L., Iacono, V. J., Krost, S. P., and Pollock, J. J. (1984) *Infect. Immun.* **44,** 695–701
9. Pollock, J. J., Denepitiya, L., MacKay, B. J., and Iacono, V. J. (1984) *Infect. Immun.* **44,** 702–707
10. Murakami, Y., Takeshita, T., Shizukuishi, S., Tsunemitsu, A., and Aimoto, S. (1990) *Arch. Oral Biol.* **35,** 775–777
11. Murakami, Y., Tamagawa, H., Shizukuishi, S., Tsunemitsu, A., and Aimoto, S. (1992) *FEMS Microbiol. Lett.* **98,** 201–204
12. Murakami, Y., Nagata, H., Amano, A., Takagaki, M., Shizukuishi, S., Tsunemitsu, A., and Aimoto, S. (1991) *Infect. Immun.* **59,** 3284–3286
13. Santarpia, R. P., III, Cho, M.-I., and Pollock, J. J. (1990) *Oral Microbiol. Immunol.* **5,** 226–232
14. Santarpia, R. P., III, Xu, L., Lal, K., and Pollock, J. J. (1992) *Oral Microbiol. Immunol.* **7,** 38–43
15. Xu, T., Levitz, S. M., Diamond, R. D., and Oppenheim, F. G. (1991) *Infect. Immun.* **59,** 2549–2554
16. Oppenheim, F. G., Yang, Y. C., and Troxler, R. F. (1985) *J. Dent. Res.* **64,** 238
17. MacKay, B. J., Pollock, J. J., Iacono, V. J., and Baum, B. J. (1984) *Infect. Immun.* **44,** 688–694
18. Oppenheim, F. G., Xu, T., McMillan, F. M., Levitz, S. M., Diamond, R. D., Offner, G. D., and Troxler, R. F. (1988) *J. Biol. Chem.* **263,** 7472–7477
19. Xu, T., Telser, R. F., Troxler, R. F., and Oppenheim, F. G. (1990) *J. Dent. Res.* **69,** 1717–1723
20. Xu, T., and Oppenheim, F. G. (1992) *J. Dent. Res.* **71,** 305
21. Lal, K., Xu, L., Colburn, J., Hong, A. L., and Pollock, J. J. (1992) *Arch. Oral Biol.* **37,** 7–13
22. vanderSpek, J. C., Offner, G. D., Troxler, R. F., and Oppenheim, F. G. (1990) *Arch. Oral Biol.* **35,** 137–143
23. Raj, P. A., Edgerton, M., and Levine, M. J. (1990) *J. Biol. Chem.* **265,** 3898–3905
24. Bevins, C. L., and Zasloff, M. (1990) *Annu. Rev. Biochem.* **59,** 395–414
25. Kagan, B. L., Selsted, M. E., Ganz, T., and Lehrer, R. I. (1990) *Proc. Natl. Acad. Sci. U. S. A.* **87,** 210–214
26. Lear, J. D., Wasserman, Z. R., and Degrado, W. F. (1988) *Science* **240,** 1177–1181

27. Miyata, T., Tokunaga, F., Yoneya, T., Yoshikawa, K., Iwanaga, S., Niwa, M., Takao, T., and Shimonishi, Y. (1989) *J. Biochem (Tokyo)* **106,** 663–668
28. States, D. J., Haberkorn, R. A., and Ruben, D. J. (1982) *J. Magn. Reson.* **48,** 286–292
29. Kumar, A., Ernst, R. R., and Wüthrich, K. (1980) *Biochem. Biophys. Res. Commun.* **64,** 2229–2246
30. Eich, G., Bodenhausen, G., and Ernst, R. R. (1982) *J. Am. Chem. Soc.* **104,** 3731–3732
31. Braunschweiler, L., and Ernst, R. R. (1983) *J. Magn. Reson.* **53,** 521–528
32. Braunschweiler, L., Kogler, H., and Ernst, R. R. (1984) *J. Magn. Reson.* **47,** 328–330
33. Davis, D. G., and Bax, A. (1985) *J. Am. Chem. Soc.* **107,** 2820–2821
34. Rance, M., and Wright, P. E. (1986) *J. Magn. Reson.* **66,** 372–378
35. Wüthrich, K. (1986) *NMR of Proteins and Nucleic Acids*, John Wiley & Sons, New York
36. Pardi, A., Wagner, G., and Wüthrich, K. (1983) *Eur. J. Biochem.* **137,** 445–454
37. Wüthrich, K., Billeter, M., and Braun, W. (1983) *J. Mol. Biol.* **169,** 949–961
38. Clore, G. M., Niges, M., Sukumaran, D. K., Brünger, A. T., Karplus, M., and Gronenborn, A. M. (1986) *EMBO J.* **5,** 2729–2735
39. Epand, R. M., Gawish, A., Iqbal, M., Guptta, K. B., Chen, C. H., Segrest, J. P., and Anantharamaiah, G. M. (1987) *J. Biol. Chem.* **262,** 9389–9396
40. Dyson, H. J., and Wright, P. E. (1991) *Annu. Rev. Biophys. Biophys. Chem.* **20,** 519–538
41. Bystrov, V. F. (1976) *Prog. NMR Spectrosc.* **10,** 41–81
42. Iqbal, M., and Balaram, P. (1981) *Biochemistry* **20,** 7278–7284
43. Rose, G. D., Gierasch, L. M., and Smith, J. A. (1985) *Adv. Protein Chem.* **37,** 1–109
44. Dyson, H. J., Lerner, R. A., and Wright, P. E. (1988) *Annu. Rev. Biophys. Biophys. Chem.* **17,** 305–324
45. Dyson, H. J., Rance, M., Houghten, R., Wright, P. E., and Lerner, R. A. (1988) *J. Mol. Biol.* **201,** 201–217
46. Raj, P. A., Das, M. K., and Balaram, P. (1988) *Biopolymers* **27,** 683–701
47. Raj, P. A., Soni, S.-D., Ramasubbu, N., Bhandary, K. K., and Levine, M. J. (1990) *Biopolymers* **30,** 73–85
48. Ravi, A., Prasad, B. V. V., and Balaram, P. (1983) *J. Am. Chem. Soc.* **105,** 105–109
49. Vijayakumar, E. K. S., and Balaram, P. (1983) *Tetrahedron* **39,** 2725–2731
50. Raj, P. A., and Balaram, P. (1985) *Biopolymers* **24,** 1131–1146
51. Wüthrich, K. (1976) *NMR in Biological Research: Peptides and Proteins*, North Holland, Amsterdam
52. Kessler, H. (1982) *Angew. Chem. Int. Ed. Engl.* **21,** 512–513
53. Greenfield, N., and Fasman, G. D. (1969) *Biochemistry* **8,** 4108–4116
54. Jung, G., Dubischar, N., and Leibritz, D. (1975) *Eur. J. Biochem.* **54,** 395–409
55. Mayr, W., Oekonomopulos, R., and Jung, G. (1979) *Biopolymers* **18,** 425–430
56. Oekonomopulos, R., and Jung, G. (1980) *Biopolymers* **19,** 203–214
57. Sudha, T. S., Vijayakumar, E. K. S., and Balaram, P. (1983) *Int. J. Peptide Protein Res.* **22,** 464–468
58. Raj, P. A., Johnsson, M., Levine, M. J., and Nancollas, G. H. (1992) *J. Biol. Chem.* **267,** 5968–5976
59. Vijayakumar, E. K. S., Sudha, T. S., and Balaram, P. (1984) *Biopolymers* **23,** 877–886
60. Kennedy, D. K., Crisma, M., Toniolo, C., and Chapman, D. (1991) *Biochemistry* **30,** 6541–6548
61. Willard, H., Merrist, L., Jr., Dean, J., and Settle, F., Jr. (1981) *Instrumental Methods of Analysis*, Wadsworth Publishing Company, Belmont, CA
62. Swedberg, S. A., Pesek, J. J., and Fink, A. L. (1990) *Anal. Biochem.* **186,** 153–158
63. Miller, B. E., Danielson, N. D., and Katon, J. E. (1988) *Appl. Spectrosc.* **42,** 401–405
64. Strand, S. W., and Jacobson, R. J. (1991) *Am. Lab.* **23,** 28–31
65. Krimm, S., and Bandekar, J. (1986) *Adv. Protein Chem.* **38,** 181–364
66. Gysin, B., and Schwyzer, R. (1983) *FEBS Lett.* **158,** 12–16
67. Jellicks, L. A., Broido, M. S., and Becker, J. M. (1989) *Biochemistry* **28,** 4233–4240
68. Milon, A., Miyazawa, T., and Higashijima, T. (1990) *Biochemistry* **29,** 65–75
69. Edgerton, M., Lo, S. E., and Levine, M. J. (1993) *J. Dent. Res.* **72,** 322
70. Dalbey, R. E. (1990) *Trends Biochem. Sci.* **15,** 253–257
71. IUPAC-IUB Commission on Biochemical Nomenclature (1968) *Biochemistry* **7,** 2703–2705